3D Tight Sandstone Digital Rock Reconstruction with Deep Learning

Jiuyu Zhao[1,1], Fuyong Wang[1,1], and Jianchao Cai[2,2]

[1]China University of Petroleum, Beijing
[2]China University of Petroleum (Beijing)

November 30, 2022

Abstract

Tight oil and gas reservoirs have attracted an increasing amount of attentions and have become one of the focus of research field in recent years. Tight sandstones have complex pore structures and narrow pores and throats with pore sizes varying from nanometers to micrometers, and studying flow mechanisms in tight sandstones is of great importance to tight oil/gas reservoir development. Reconstructing digital rock, which can comprehensively represent the petrophysical properties of tight sandstone, is key to simulating the fluid flow in micro/nanopores. This paper proposes a new method of reconstructing 3D digital rock from CT images of tight sandstones based on a deep convolutional generative adversarial network (DCGAN), and 3D convolution in the generator and discriminator are adopted to realize reconstruction from 1D data to a 3D digital rock model. The model adopts pore area, volume, spatial distribution and connectivity, Fréchet inception distance score to evaluate the proposed model. Studies show that when the training effect is slightly poor, the generated digital rock model will exhibit noise, which can be reduced by postprocessing; when the training effect is good, DCGAN can accurately reconstruct the 3D digital rock model of tight sandstones, and the reconstructed digital rock is very consistent with the pore size, geometric structure, and connectivity of natural tight sandstones. When multiple 3D tight sandstone CT images are used for training, the DCGAN can learn the pore structure characteristics of entire tight sandstone bodies, which have strong heterogeneous, and the porosity distribution obtained from the generated digital rock is similar to that of the original tight sandstone.

1   Fuyong Wang (Orcid ID: 0000-0003-1202-5283)
2   Jiuyu Zhao (Orcid ID: 0000-0001-9867-1395)
3   Jianchao Cai (Orcid ID:0000-0003-2950-888X)
4
5

6   **3D Tight Sandstone Digital Rock Reconstruction with Deep Learning**

7

8   **Jiuyu Zhao[1], Fuyong Wang[1, 2, *], Jianchao Cai[1]**

9

10   [1] *State Key Laboratory of Petroleum Resources and Prospecting, China University of Petroleum* (*Beijing*),
11   *Beijing 102249*

12   [2] *Unconventional Petroleum Research Institute, China University of Petroleum* (*Beijing*) *Beijing 102249*

13   Corresponding author: Fuyong Wang (wangfuyong@cup.edu.cn)

14

15   **Key Points:**

16   • Reconstructing 3D heterogeneous tight sandstone digital rock based on DCGAN with 3D
17   convolution used in the generator and the discriminator.

18   • A more comprehensive method for evaluating reconstructed 3D digital rock with strong
19   heterogeneity is adopted.

20   • The reconstructed 3D digital rock has the similar porosity distribution with the original
21   heterogeneous tight sandstone.
22

Abstract

Tight oil and gas reservoirs have attracted many attentions and are one of the hottest research fields in recent years. Tight sandstones have complex pore structures and narrow pores and throats with pore sizes varying from nanometers to micrometers, studying flow mechanisms in tight sandstones is of significance to tight oil/gas reservoir development. Reconstructing the digital rock which can comprehensively represent petrophysical properties of tight sandstone is the key to simulate the fluid flow in micro/nano pores. This paper proposes a new method of reconstructing 3D digital rock from CT image of tight sandstones based on a deep convolutional generative adversative network (DCGAN), and 3D convolution in the generator and discriminator are adopted to realize reconstruction from one dimensional data to 3D digital rock model. Studies show that when the training effect is slightly poor, the generated digital rock model will have noise, which can be reduced by post-processing; when the training effect is well, DCGAN can accurately reconstruct the 3D digital rock of tight sandstones, the reconstructed digital rock is very consistent in pore size, geometric structure, and connectivity of natural tight sandstones. When multiple 3D tight sandstone CT images are used for training, the DCGAN can learn the pore structure characteristics of entire tight sandstones, and the porosity distribution obtained from generated digital rock are similar to original tight sandstones.

Keywords: digital rock; tight sandstone; generative adversarial neural network; deep learning

1 Introduction

Unconventional oil and gas are important alternative energy in the future (Jia, 2017). Tight oil/gas reservoirs in China are mainly continental deposits, and a great deal of micro and nano-pores are widely developed with poor connections, complex structures and strong heterogeneity (Yao et al., 2013; Li et al., 2017; Wang et al., 2019) , therefore, the seepage mechanisms in tight oil/gas reservoirs are quite complicated. It is necessary to study the microscopic flow mechanism and figure out its influencing factors for developing the tight oil/gas reservoirs efficiently and economically. Digital rock is an advanced technology to study the physical properties and flow behaviors insides of sedimentary rock (Berg et al., 2017), which will play an important role in the exploration and development of tight oil/gas reservoirs.

In order to investigate the characteristics of sedimentary rock, the key is constructing a 3D digital rock model which can accurately characterize the pore structure of micro and nano-pores. At present, the methods of 3D digital rock reconstruction can be divided into two main categories: physical experiments and numerical reconstructions (Yao et al., 2013). Physical experiments have to use a high-resolution scanning instruments, these methods are time consuming with high cost (Izadi et al., 2017). The common physical experiments methods includes serial sectioning, magnetic resonance imaging (MRI) (Ouellette et al., 2015), X-ray computed tomography (Elbakri and Fessler, 2002), focused ion beam (FIB)-scanning electron microscopy (SEM) (Bera et al., 2011), and etc. Numerical reconstruction method reconstructs digital rock with computer based on the statistical information of pore structures, and can be divided into two categories: random field method and process-based method (Øren and Bakke, 2002). The random field method also has multiple types, including Gaussian random field method(Yuan et al., 2010), simulated annealing method (Yeong and Torquato, 1998), Markov chain Monte Carlo Method (Wu et al., 2004), sequential indicator simulation method (Keehm et al., 2004) and multiple-point statistics method(Lei, 2020), and etc.

Recently, artificial intelligent has been gradually widely applied in oil industry, including seismic data processing and interpretation (Cao and Wu, 2017; Imamverdiyev and Sukhostat, 2019), well drilling (Chen et al., 2019; Noshi and Schubert, 2018), oil and gas exploitation (Ahmadi and Chen, 2019; Li et al., 2019). It is a trend that the whole oil industry will pay more attentions on intelligent system development. Generative adversarial networks (GAN) is a neural network model proposed by Goodfellow et al. (Goodfellow et al., 2014), which can capture the distribution of data and generate a data sample consistent with the distribution of real data. The main ideal of GAN is derived from the zero-sum game in game theory, the generator can learn the distribution of data through the continuous game between the generator and the discriminator, which can produce an output that is more consistent with real data. It has been widely used in intelligent fusion(Ma et al., 2019), intelligent generating(Wang et al., 2018), super-resolution reconstruction(Bulat et al., 2018), classification(Zhou et al., 2018), etc. It also has been used in the construction of 3D psychical models, such as face model (Gecer et al., 2019; Gecer et al., 2019), bed/chair/table model (Li et al., 2019), archaeological objects (Hermoza and Sipiran, 2018).

As mentioned above, the GAN provides a new method for digital rock reconstruction, and different GAN model has been used in digital rock reconstruction. Mosser et al (Mosser et al., 2017; Mosser et al., 2018) firstly introduced GAN to reconstruct digital rock. They generated a 3D digital rock model ($64\times64\times64$) , and used autocorrelation function to evaluate the reconstructed digital rock, but the process of model training is time consuming. DCGAN adapts the convolutional neural network (CNN) as the generator and discriminator, which is very good at dealing with image processing problem (Radford et al., 2015). In 2018, Guan (2018) used DCGAN to generate 2D images rather than 3D models, and another GAN model, Wasserstein GAN (Arjovsky et al., 2017), was introduced for comparison in their presentation. Liu et al.(Liu et al., 2019)used Berea sandstone ($64\times64\times64$) and Estaillades carbonate ($128\times128\times128$) binary data respectively to train DCGAN model and for 3D digital rock reconstruction; Shams et al.(2020) coupled GAN and auto-encoder neural network (AE) for reconstructing a porous media with inter-grain and intra-grain pores. The function of GAN is producing 3D porous media ($64\times64\times64$) with inter-grain pores, and the AE (256×256) is to generate intra-grain pore in the images outputted from the GAN. Valsecchi et al.(Valsecchi et al., 2020)designed the generator with 3D convolution and the discriminator with 2D convolution for generating a 3D model with 2D image stacks output (64×64), and three types of brainy image data was used to validate the model by two-point probability function and Minkowski functionals. The conditional generative confrontation network (CGAN) (Mirza and Osindero, 2014), which adds constraints to the original GAN by introducing a conditional variable 'y' into the generative model and the discriminant model to guide the generation of data, is another model for digital rock reconstruction. Feng et al.(2019a; 2019b) applied CGAN to reconstruct complete 2D core images (128×128) based on less information of images and real core data. Volkhonskiy et al.(2019)added autoencoders before the generator of CGAN to extract pore structure information and input it to the generator as constraints, and different natural core samples were used to evaluate its performance but the consuming time of generative model training is about 10 hours.

Digital rock reconstruction with GAN is an emerging technology, there are many challenges need to overcome, such as a long training time, complex model, small size of generated model, and representativeness, generalization ability and interpretability are still weak. In this paper, a new method of digital rock reconstruction based on DCGAN is developed, and the 3D convolution networks are adopted in the generator and discriminator of DCGAN. The CT

112 images of tight sandstones form Yanchang formation, Ordos Basin, NW China are used to
113 validate the newly proposed model. The geometry and connectivity of pores in the reconstructed
114 digital rocks are analyzed with three case studies.

115

116 **2 Methodology**

117 2.1 GAN

118 As a classical unsupervised learning model, GAN combines the game theory and deep
119 neural network, has some advantages those generative models don't have. It avoids inference
120 during training, and can produce a clearer sample. If the discriminator is well trained, the
121 generator can learn the distribution of data perfectly in theory by training. The value function of
122 GAN $V(D,G)$ is defined as (Goodfellow et al., 2014):

123
$$\min_G \max_D V(D,G) = E_{x \sim p_{data}(x)}\Big[\log D(x)\Big] + E_{z \sim p_z(z)}\Big[\log\big(1 - D\big(G(z)\big)\big)\Big] \tag{1}$$

124 where x is the real data; z is the noise; $p_{data}(x)$ is the distribution of real data; $p_z(z)$ is the
125 distribution of noise; $G(z)$ is the output of generator; $D(x)$ represents the probability that x is
126 real data judged by the discriminator.

127 In the training process, backpropagation algorithm is used to optimize the parameters of
128 network. When the distribution of real data and the distribution of generator is equal, the value
129 function is the lowest, and the generative model can perfectly learn the data distribution. In order
130 to avoid the generator falling into local minima, the discriminator will train several times while
131 the generator updates once.

132 DCGAN scales up GAN using CNN, and three changes were made to the structure and
133 activation function of CNN. First, the pooling layer in conventional CNN is replaced by
134 convolution. Then, the generator uses ReLU activation for all layers except the output layer,
135 which uses tanh activation, but the discriminator uses Leaky ReLU activation in all layers.
136 Finally, both the generator and the discriminator apply batch normalization for stabilizing
137 training.

138 2.2 Network architecture

139 The schematic diagram of applying DCGAN for 3D digital rock reconstruction is shown
140 in **Figure 1**, and the detail parameters of discriminator and generator are shown in **Table 1**.

141 The discriminator is a CNN model to discriminate the input data is real data or the data
142 from generator. It has four convolutional layers, and each convolutional layer consists of a batch
143 normalization layer with momentum of 0.8, a drop layer with loss ratio of 0.25, and the Leaky
144 ReLU with activation of 0.2. The last layer is a fully connect layer, its activation is sigmoid
145 function. The structure of discriminator is shown in **Figure 2**.

146 The generator receives a random noise conforming to normal distribution, and converts
147 the random noise to a 1D vector by a fully connect layer, then reshapes the random noise to a
148 four-dimensional vector. Three up sampling layers are used to enlarge the 3D images, the
149 followed convolutional layer of each up sampling layer can learn the kernel by training, and then
150 the data flows into batch normalization layer and ReLU activation. The last layer is a

151 convolutional layer, and the activation function is tanh function. The momentum of batch
152 normalization layer is set to 0.8. The structure of the generator used in this manuscript is shown
153 in **Figure 3**.

154 **3 Data and plateform**

155   3.1 Data sets

156   As shown in **Figure 4**, the Micro XCT-510 scanner was used to obtain the CT images of
157 tight sandstones Yanchang formation, Ordos Basin, NW China. The resolution of CT images is
158 1.22 μm.

159   There are always some noises in the CT images due to the influence of equipment,
160 environment, and the minerals of the rock itself. The image noises have significant influences on
161 pore structure analysis, thus the image preprocessing must be conducted. The common methods
162 of image denoising includes Gaussian filter, median filter, adaptive Wiener filter, mean filtering,
163 and wavelet thresholding(Buades et al., 2005; Zhang and Desai, 2002). Here the median filter
164 was used to remove the noise in CT images. After that, the images will be divided into pore and
165 matrix two parts, and binary image can reduce the calculation time comparing with grey images.

166   Considering the calculation ability of our computer, the data for training was sub-
167 sampled from the binary CT images. Binary CT images for training ($32\times32\times910$) are shown in
168 **Figure 5**, the black is the pore and the gray is the matrix. According to the statistics of porosity
169 of 910 core slices, the binary images with porosity less than 10% account for 60% of total CT
170 images, indicating that most pores are small pores, which reflects strong heterogeneity of tight
171 sandstone pore structures. The 2D images must to be transform into 3D data, and the
172 normalization of binary data (0~255) also are also needed. The range of data after normalization
173 is between -1 and 1 because the distribution of the tanh function ranges from -1 to 1.

174   3.2 Platform

175   Several platforms have been developed for machine learn, such as Tensorflow (Abadi et
176 al., 2016), Keras (Gulli and Pal, 2017), Caffe (Jia et al., 2014), Pytorch (Paszke et al., 2017),
177 Theano(Al-Rfou et al., 2016). In this paper, Keras is used to build the DCGAN model, which is
178 an advanced neural network API written in Python and be coupled with Tensorflow or Theano as
179 the backend. As the network has a complex structure and needs a large amount of calculation, the
180 configuration of computer will have a great impact on the training and application of deep
181 learning. A computer with a single NVIDIA GTX 1050 GPU was used in this paper.

182 **4 Results and discussion**

183   4.1 Case 1

184   The input data is 3D binary image with the size of $32\times32\times32$, and the value function of
185 the generator and the discriminator are optimized by Adam method. The learning rate is set to
186 0.002, the exponential decay rate for the moment estimation is 0.5, the number of training epoch
187 is 6000, and the batch data size is 1. The generated digital rock by is shown in **Figure 6**.
188 Compared with the original digital rock, the generated digital rock has similar pores, but some
189 isolated pores are also generated. Compared 9 pores in the original digital rock, there are 30
190 pores in the generated digital rock. **Figure 7** shows the distribution of pore area and pore volume

191 of original digital rock and generated digital rock, which can be found that most of pores in the
192 generated digital rock is the small pores.

193 Removing all the isolated small pores with the pore volume less than 5 μm^3 in the
194 generated digital rock, only 9 large pores are left, which are same to the pores in the original
195 digital rock. As shown in **Table 2**, the barycenter coordinates of the pores in the generated digital
196 rock are very close to those in original rock, except for the pores nos. 1, 6, and 7. For other pores,
197 the distances between the generated pores and original pores are less than 1 μm. In addition, the
198 distributions of pore volumes and pore areas in the original digital rock and generated digital
199 rock are very close, as shown in **Figure 8**.

200 Two-point probability function can reflect the pore distribution insides of digital rock. As
201 shown in **Figure 9**, the curves of two-point probability functions of the original digital rock and
202 generated digital rock are very close to each other, which can demonstrate that the method of
203 digital rock reconstruction based on deep learning is reliable, and can accurately reconstruct
204 digital rock. The porosity of original rock and generated digital rock is about 4.5%, but the
205 porosity of generated digital rock is a little higher, due to there are several isolated small pores in
206 the generated digital rock. Even that, the reconstructed digital rock by deep learning can
207 accurately represent the original digital rock.

208 4.2 Case 2

209 The input data is another 3D binary images with size of 32×32×32, and the original
210 digital rock is shown in **Figure 11(a)**. Using the parameters of DCGAN obtained from training
211 above, the generated digital rock reconstructed by deep learning is shown in **Figure 11(b)**. As
212 shown in **Table 4**, the barycenter coordinates of the pores in the original digital rock and
213 generated digital rock are the same.

214 As shown in **Figure 11**, the porosity of the original digital rock and generated digital rock
215 is 46.8%, and the curves of two-point probability functions of the original digital rock and
216 generated digital rock coincide. It could be concluded that a well-trained DCGAN can generate
217 the same digital rock as the original input dataset.

218 4.3 Case 3

219 Different from only 32 slices of CT images used in case 2, total 910 slices of CT images
220 are used for training DCGAN. The initial parameters for GCGAN are same to those in cases 1
221 and 2, except the batch size in case 3 is 4 rather than 1. It means that four digital rocks with the
222 size of 32×32×32 are used as the input data for DCGAN training, and also four digital rock with
223 the size are generated. **Figure 13** shows the four digital rocks generated by DCGAN after
224 training. As the original digital rock with the size of 32×32×910 has strong heterogeneity, and
225 the size of generated digital rock is different from the original digital rock, the two-point
226 probability function is not suitable for comparing the difference of pore size distribution between
227 generated digital rock and original digital rock. As shown in **Figure 13**, the distribution of area
228 porosity in 2D images of the four generate digital rocks (32×4 slices) is similar to that in the
229 original digital rock (910 slices). The images with porosity between 0% and 10% both account
230 for about 60% of total images, and the small pores account for a larger proportion.

5 Conclusions

This paper proposed a new method of reconstructing 3D digital rock based on deep learning, and the DCGAN with 3D convolution in generator and discriminator is built for 3D digital rock reconstruction. The reconstructed digital rock is evaluated by the statistical results of pore size distribution and two-point probability function. The results show when DCGAN is well trained, it can generate a representative digital rock similar to original one. When the DCGAN is not well trained, the post processing such as image filtering can improve the accuracy of digital rock reconstruction. The well-trained DCGAN can generate the digital rock with different pore structures, but the porosity distribution is similar to the original digital rock. The reconstructed digital rock is helpful for study the characteristics of pore structures and flow mechanism insides of porous media. The future work can focus on improving the accuracy of reconstructed digital rock, reducing training time, strengthening model generalization ability, and model explanation and evaluation.

References

Abadi, M. et al., 2016. Tensorflow: Large-scale machine learning on heterogeneous distributed systems. *arXiv preprint* arXiv:1603.04467.

Ahmadi, M.A. and Chen, Z., 2019. Machine learning models to predict bottom hole pressure in multi-phase flow in vertical oil production wells. *The Canadian Journal of Chemical Engineering*, 97(11): 2928-2940. https://doi.org/10.1002/cjce.23526

Al-Rfou, R. et al., 2016. Theano: A Python framework for fast computation of mathematical expressions. *arXiv e-prints*: arXiv: 1605.02688.

Arjovsky, M., Chintala, S. and Bottou, L., 2017. Wasserstein gan. *arXiv preprint* arXiv:1701.07875.

Bera, B., Mitra, S.K. and Vick, D., 2011. Understanding the micro structure of Berea Sandstone by the simultaneous use of micro-computed tomography (micro-CT) and focused ion beam-scanning electron microscopy (FIB-SEM). *Micron*, 42(5): 412-418. https://doi.org/10.1016/j.micron.2010.12.002

Berg, C.F., Lopez, O. and Berland, H., 2017. Industrial applications of digital rock technology. *Journal of Petroleum Science and Engineering*, 157: 131-147. https://doi.org/10.1016/j.petrol.2017.06.074

Buades, A., Coll, B. and Morel, J., 2005. A review of image denoising algorithms, with a new one. *Multiscale Modeling & Simulation*, 4(2): 490-530. https://doi.org/10.1137/040616024

Bulat, A., Yang, J. and Tzimiropoulos, G., 2018. To learn image super-resolution, use a gan to learn how to do image degradation first, *Proceedings of the European conference on computer vision (ECCV)*, pp. 185-200.

Cao, J. and Wu, S., 2017. Deep Learning: Chance and Challenge for Deep Gas Reservoir

274   *IdentificationInternational Geophysical Conference, Qingdao, China, 17-20 April 2017*, pp.
275   711-712. https://doi.org/10.1190/IGC2017-180

276 Chen, W., Yu, Y., Shen, Y., Zhang, Z. and Vesselinov, V., 2019. Automatic Drilling Dynamics
277   Interpretation Using Deep Learning, *SPE Annual Technical Conference and Exhibition*.
278   Society of Petroleum Engineers. https://doi.org/10.2118/195919-MS

279 Elbakri, I.A. and Fessler, J.A., 2002. Statistical image reconstruction for polyenergetic X-ray
280   computed tomography. *IEEE transactions on medical imaging*, 21(2): 89-99. doi:
281   10.1109/42.993128

282 Feng, J. et al., 2019a. Reconstruction of porous media from extremely limited information using
283   conditional generative adversarial networks. *Physical Review E*, 100(3): 033308.
284   https://doi.org/10.1103/PhysRevE.100.033308

285 Feng, J. et al., 2019b. Accurate and fast reconstruction of porous media from extremely limited
286   information using conditional generative adversarial network. *arXiv preprint*
287   arXiv:1905.02135.

288 Gecer, B. et al., 2019. Synthesizing coupled 3d face modalities by trunk-branch generative
289   adversarial networks. *arXiv preprint* arXiv:1909.02215.

290 Gecer, B., Ploumpis, S., Kotsia, I. and Zafeiriou, S., 2019. Ganfit: Generative adversarial
291   network fitting for high fidelity 3d face reconstruction, *Proceedings of the IEEE Conference*
292   *on Computer Vision and Pattern Recognition*, pp. 1155-1164.

293 Goodfellow, I. et al., 2014. Generative adversarial nets, *Advances in neural information*
294   *processing systems*, pp. 2672-2680.

295 Guan, K., 2018. Reconstructing Pore Networks Using Generative Adversarial Networks.
296   http://cs229.stanford.edu/proj2018/report/222.pdf

297 Gulli, A. and Pal, S., 2017. Deep learning with Keras. *Packt Publishing Ltd*.

298 Hermoza, R. and Sipiran, I., 2018. 3D Reconstruction of incomplete archaeological objects using
299   a generative adversarial network. *Proceedings of Computer Graphics International 2018*,
300   pp. 5-11. https://doi.org/10.1145/3208159.3208173

301 Imamverdiyev, Y. and Sukhostat, L., 2019. Lithological facies classification using deep
302   convolutional neural network. Journal of Petroleum Science and Engineering, 174: 216-228.
303   https://doi.org/10.1016/j.petrol.2018.11.023

304 Izadi, H. et al., 2017. Application of full set of two point correlation functions from a pair of 2D
305   cut sections for 3D porous media reconstruction. Journal of Petroleum Science and
306   Engineering, 149: 789-800. https://doi.org/10.1016/j.petrol.2016.10.065

307 Jia, C., 2017. Breakthrough and significance of unconventional oil and gas to classical petroleum
308   geology theory - ScienceDirect. Petroleum Exploration and Development, 44(1): 1-10.
309   https://doi.org/10.1016/S1876-3804(17)30002-2

310 Jia, Y. et al., 2014. Caffe: Convolutional architecture for fast feature embedding, *Proceedings of*
311   *the 22nd ACM international conference on Multimedia*, pp. 675-678.
312   https://doi.org/10.1145/2647868.2654889

313 Keehm, Y., Mukerji, T. and Nur, A., 2004. Permeability prediction from thin sections: 3D
314   reconstruction and Lattice-Boltzmann flow simulation. *Geophysical Research Letters*,
315   31(4). https://doi.org/10.1029/2003GL018761

316 Lei, Y., 2020. Reconstruction and Analysis of Tight Sandstone Digital Rock Combined with X-
317   Ray CT Scanning and Multiple-Point Geostatistics Algorithm. *Mathematical Problems in*
318   *Engineering*, 2020. https://doi.org/10.1155/2020/9476060

319 Li, H., Zheng, Y., Wu, X. and Cai, Q., 2019. 3D model generation and reconstruction using

conditional generative adversarial network. *International Journal of Computational Intelligence Systems*, 12(2): 697-705. https://doi.org/10.2991/ijcis.d.190617.001

Li, P., Zheng, M., Bi, H., Wu, S. and Wang, X., 2017. Pore throat structure and fractal characteristics of tight oil sandstone: a case study in the Ordos Basin, China. *Journal of Petroleum Science and Engineering*, 149: 665-674. https://doi.org/10.1016/j.petrol.2016.11.015

Li, Y., Sun, R. and Horne, R., 2019. Deep learning for well data history analysis, *SPE Annual Technical Conference and Exhibition*. Society of Petroleum Engineers. https://doi.org/10.2118/196011-MS

Liu, S. et al., 2019. A case study on homogeneous and heterogeneous reservoir porous media reconstruction by using generative adversarial networks. *Energy Procedia*, 158: 6164-6169. https://doi.org/10.1016/j.egypro.2019.01.493

Ma, J., Yu, W., Liang, P., Li, C. and Jiang, J., 2019. FusionGAN: A generative adversarial network for infrared and visible image fusion. *Information Fusion*, 48: 11-26. https://doi.org/10.1016/j.inffus.2018.09.004

Mirza, M. and Osindero, S., 2014. Conditional generative adversarial nets. *arXiv preprint* arXiv:1411.1784.

Mosser, L., Dubrule, O. and Blunt, M.J., 2017. Reconstruction of three-dimensional porous media using generative adversarial neural networks. *Physical review. E*, 96(4): 043309-043309. https://doi.org/10.1103/PhysRevE.96.043309

Mosser, L., Dubrule, O. and Blunt, M.J., 2018. Conditioning of three-dimensional generative adversarial networks for pore and reservoir-scale models. *arXiv preprint* arXiv:1802.05622.

Noshi, C.I. and Schubert, J.J., 2018. The role of machine learning in drilling operations; a review, *SPE/AAPG Eastern Regional Meeting*. Society of Petroleum Engineers. https://doi.org/10.2118/191823-18ERM-MS

Øren, P. and Bakke, S., 2002. Process based reconstruction of sandstones and prediction of transport properties. *Transport in porous media*, 46(2-3): 311-343.

Ouellette, M. et al., 2015. Rock Core Analysis: Metallic Core Holders for Magnetic Resonance Imaging Under Reservoir Conditions. *In Mobile NMR and MRI*, pp. 290-309.

Paszke, A. et al., 2017. Automatic differentiation in pytorch. *31st Conference on Neural Information Processing Systems (NIPS 2017)*, Long Beach, CA, USA.

Radford, A., Metz, L. and Chintala, S., 2015. Unsupervised representation learning with deep convolutional generative adversarial networks. *arXiv preprint* arXiv:1511.06434.

Shams, R., Masihi, M., Boozarjomehry, R.B. and Blunt, M.J., 2020. Coupled generative adversarial and auto-encoder neural networks to reconstruct three-dimensional multi-scale porous media. *Journal of Petroleum Science and Engineering*, 186: 106794. https://doi.org/10.1016/j.petrol.2019.106794

Valsecchi, A., Damas, S., Tubilleja, C. and Arechalde, J., 2020. Stochastic reconstruction of 3D porous media from 2D images using generative adversarial networks. *Neurocomputing*. 399, 227-236. https://doi.org/10.1016/j.neucom.2019.12.040

Volkhonskiy, D. et al., 2019. Reconstruction of 3d porous media from 2d slices. *arXiv preprint* arXiv:1901.10233.

Wang, F., Yang, K., You, J. and Lei, X., 2019. Analysis of pore size distribution and fractal dimension in tight sandstone with mercury intrusion porosimetry. *Results in Physics*, 13: 102283. https://doi.org/10.1016/j.rinp.2019.102283

Wang, H., Qin, Z. and Wan, T., 2018. Text generation based on generative adversarial nets with

latent variables, *Pacific-Asia Conference on Knowledge Discovery and Data Mining*. Springer, pp. 92-103.

Wu, K., Nunan, N., Crawford, J.W., Young, I.M. and Ritz, K., 2004. An efficient Markov chain model for the simulation of heterogeneous soil structure. *Soil Science Society of America Journal*, 68(2): 346-351. https://doi.org/10.2136/sssaj2004.3460

Yao, J. et al., 2013. Characteristics of tight oil in Triassic Yanchang formation, Ordos Basin. *Petroleum Exploration and Developmen*t, 40(2): 161-169. https://doi.org/10.1016/S1876-3804(13)60019-1

Yao, J., Wang, C., Yang, Y., Hu, R. and Wang, X., 2013. The construction of carbonate digital rock with hybrid superposition method. *Journal of Petroleum Science and Engineering*, 110: 263-267. https://doi.org/10.1016/j.petrol.2013.10.005

Yeong, C. and Torquato, S., 1998. Reconstructing random media. *Physical review E*, 57(1): 495. https://doi.org/10.1103/PhysRevE.57.495

Yuan, H., Lee, J.H. and Guilkey, J.E., 2010. Stochastic reconstruction of the microstructure of equilibrium form snow and computation of effective elastic properties. *Journal of Glaciology*, 56(197): 405-414. https://doi.org/10.3189/002214310792447770

Zhang, X.P. and Desai, M.D., 2002. Wavelet based automatic thresholding for image segmentation, *Proceedings of International Conference on Image Processing*. Vol. 1, pp. 224-227. dio: 10.1109/ICIP.1997.647744

Zhou, T., Liu, W., Zhou, C. and Chen, L., 2018. Gan-based semi-supervised for imbalanced data classification, 2018 4th International Conference on Information Management (ICIM). IEEE, pp. 17-21. dio: 10.1109/INFOMAN.2018.8392662
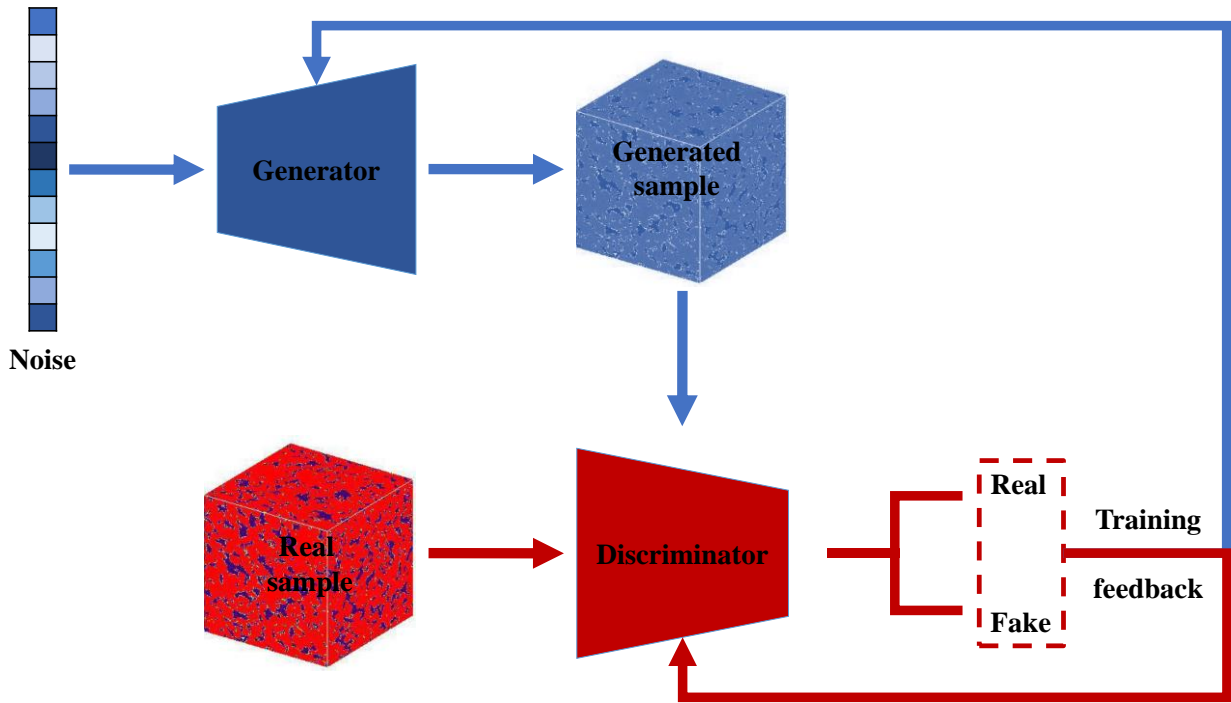
390
391   **Figure 1** The schematic diagram of 3D digital rock reconstruction with DCGAN.
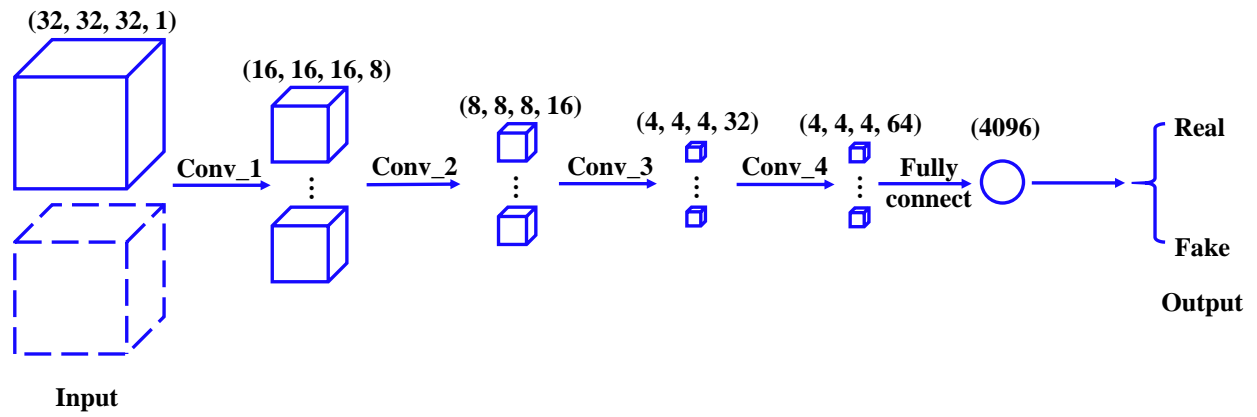392

393

394 **Figure 2** The structure of discriminator.
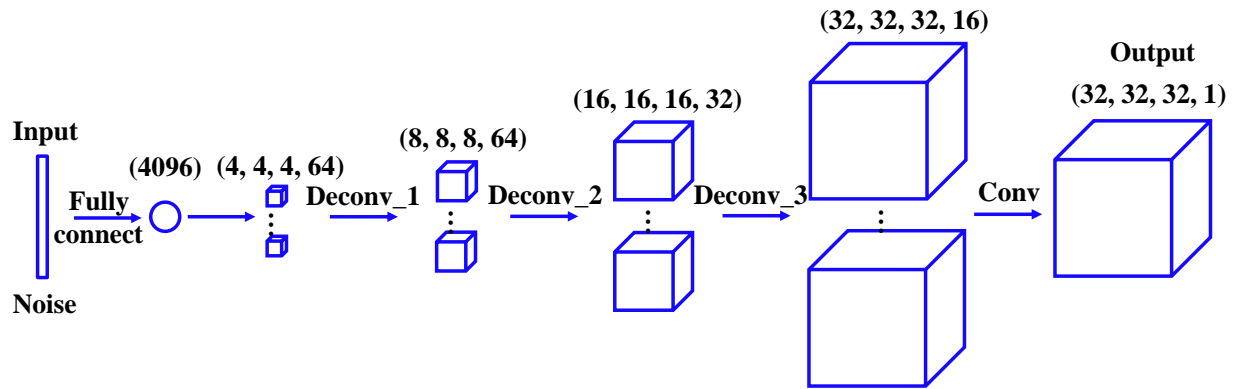
395

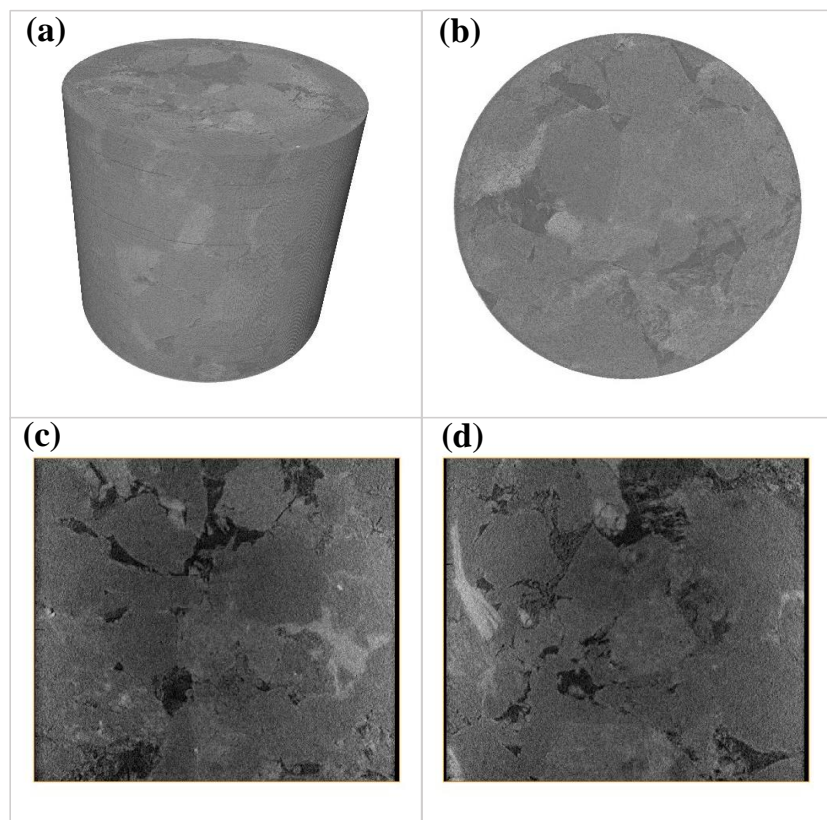**Figure 3** The structure of generator

399

Figure 4 CT images of tight sandstones from Yanchang formation, Ordos Basin, NW China ((a) 3D view of core samples, (b) CT slice in XY direction, (c) CT slice in XZ direction, (d) CT slice in YZ direction)
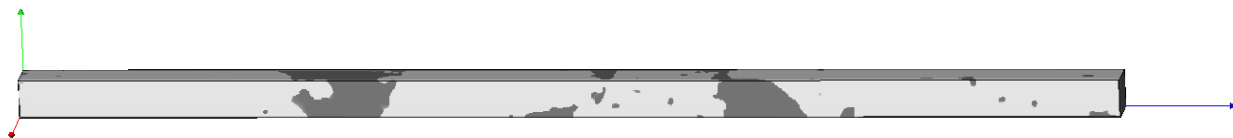
403

404

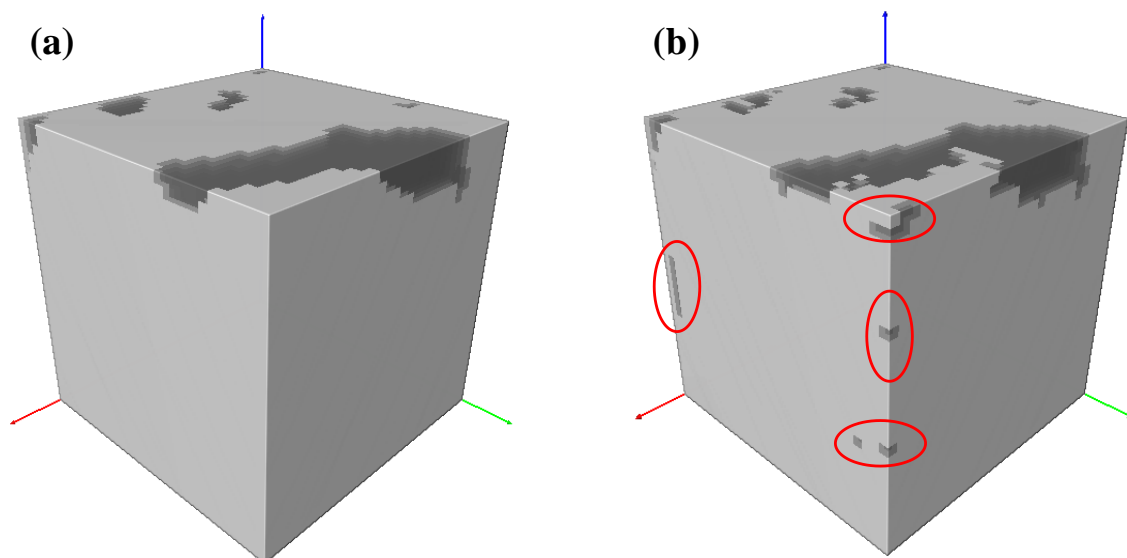**Figure 5** The binary CT images of tight sandstones for training, and the size of images are 32×32×910.

407

(a)

(b)

408

409 **Figure 6** Comparison of the original digital rock (a) and the generated digital rock reconstructed
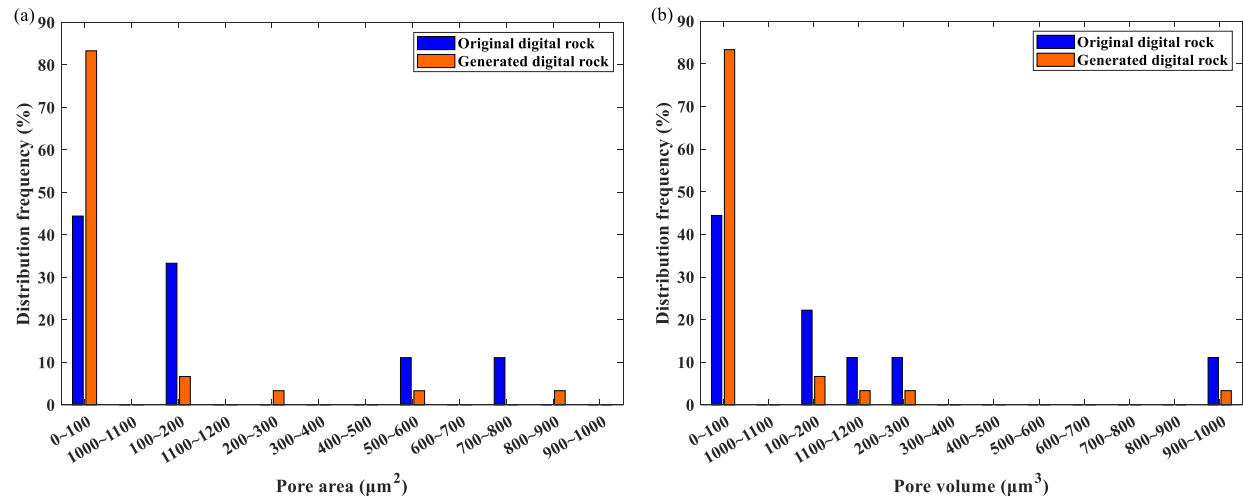410 by deep learning (b)

411

412
413 **Figure 7** Comparison of the pore area (a) and pore volume (b) in the original digital rock
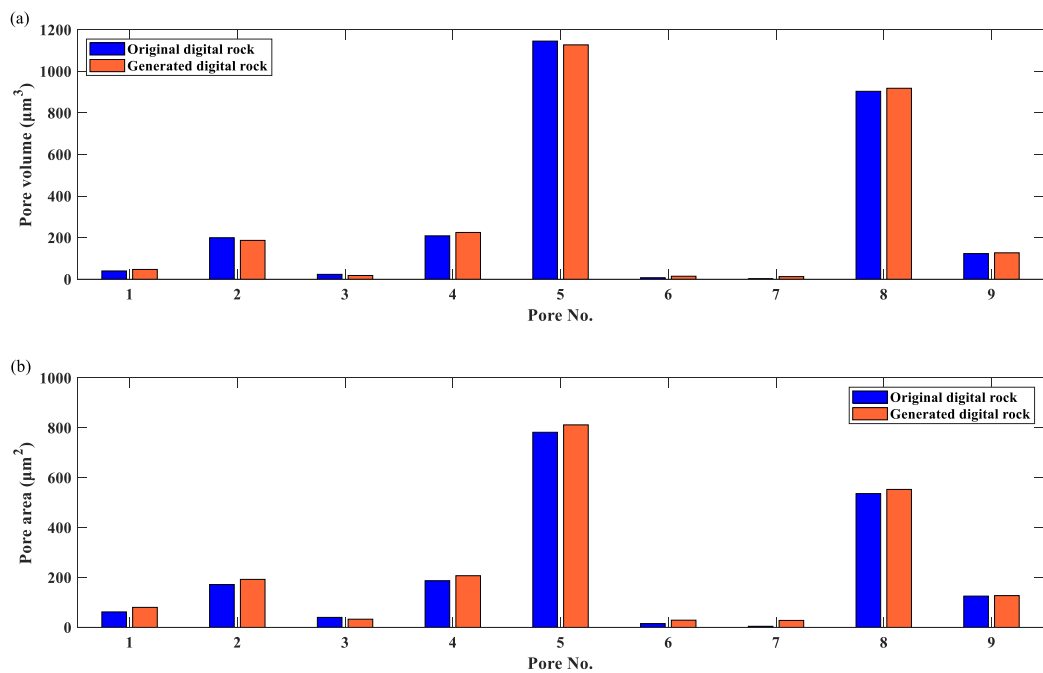414

415

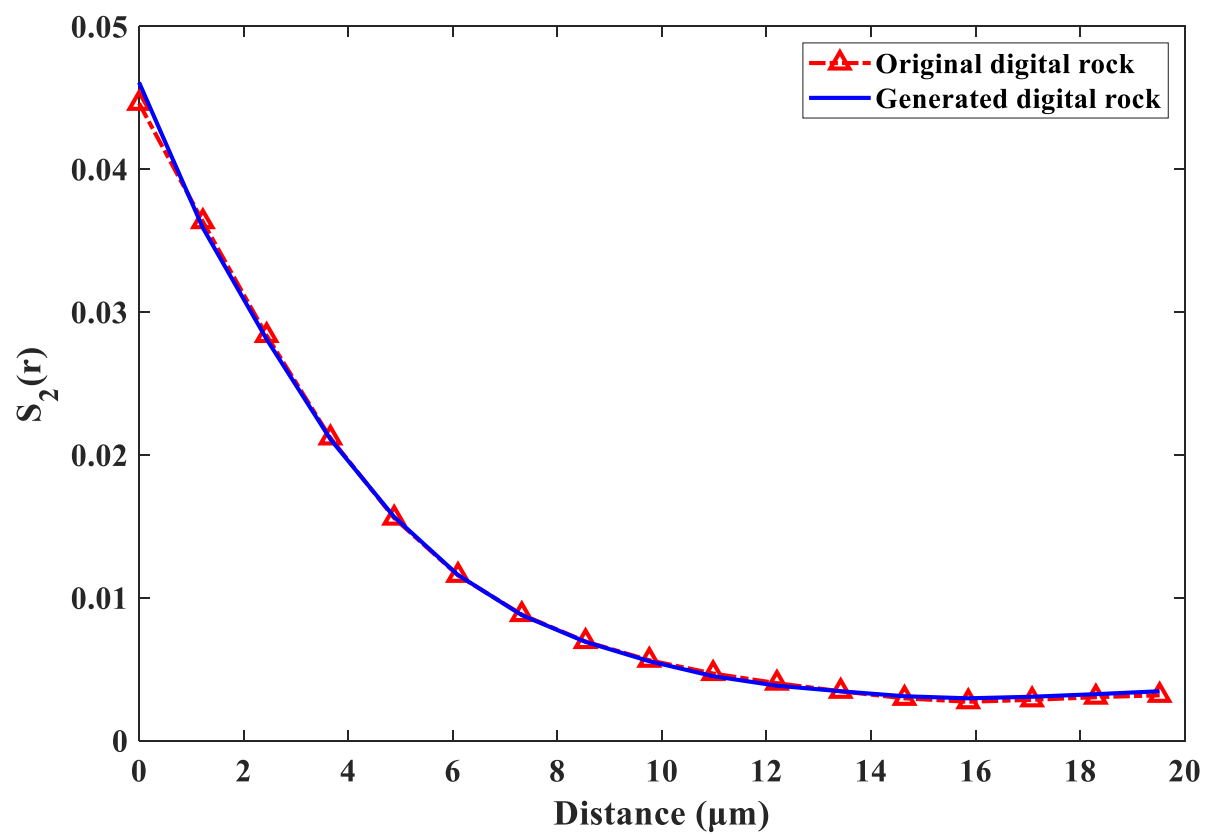416 **Figure 8** Comparison of pore volume (a) and pore area (b) in the original digital rock and
417 generated digital rock
418

419

420 **Figure 9** Two-point probability function of the original digital rock and the generated digital
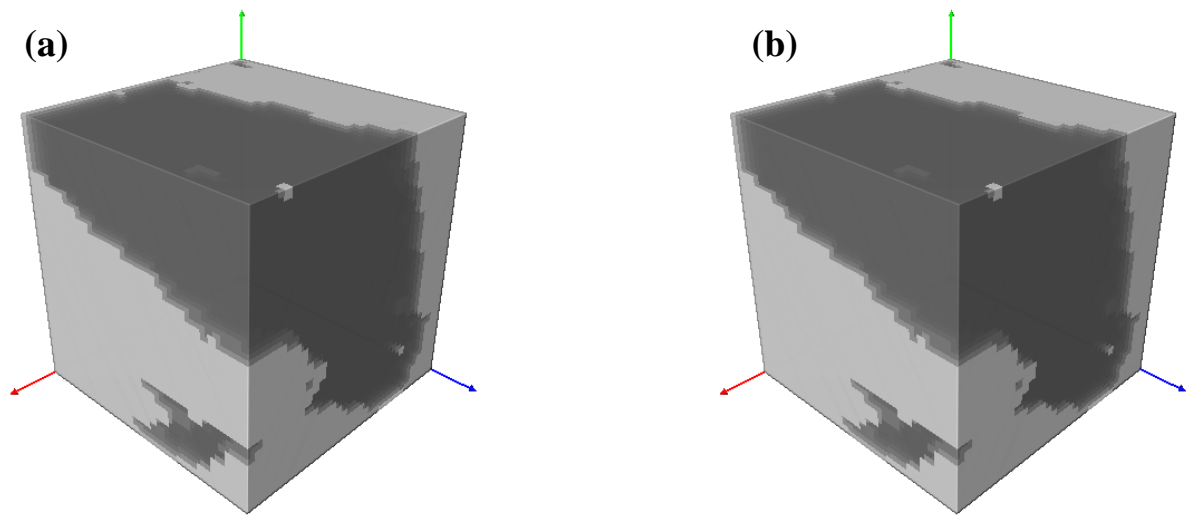421 rock after denoising.

422

423

424 **Figure 10** The original 3D digital rock (a) and the generated 3D digital rock reconstructed by
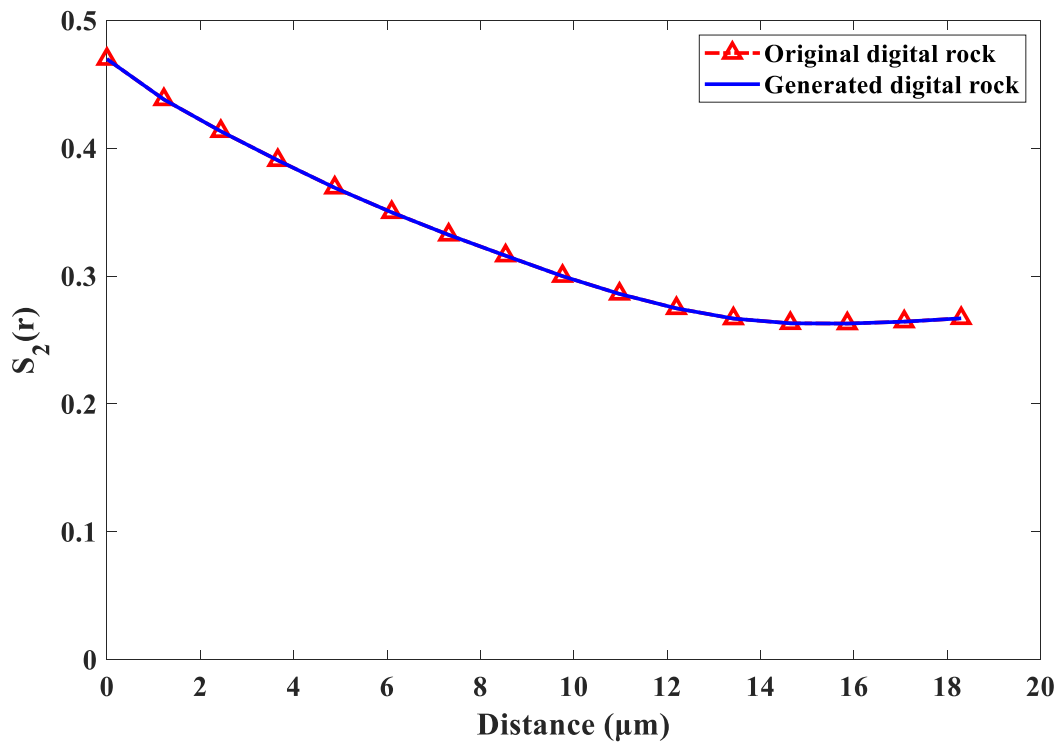425 deep learning (b)
426

427

428   **Figure 11** Two-point probability function of the original digital rock and the generated digital
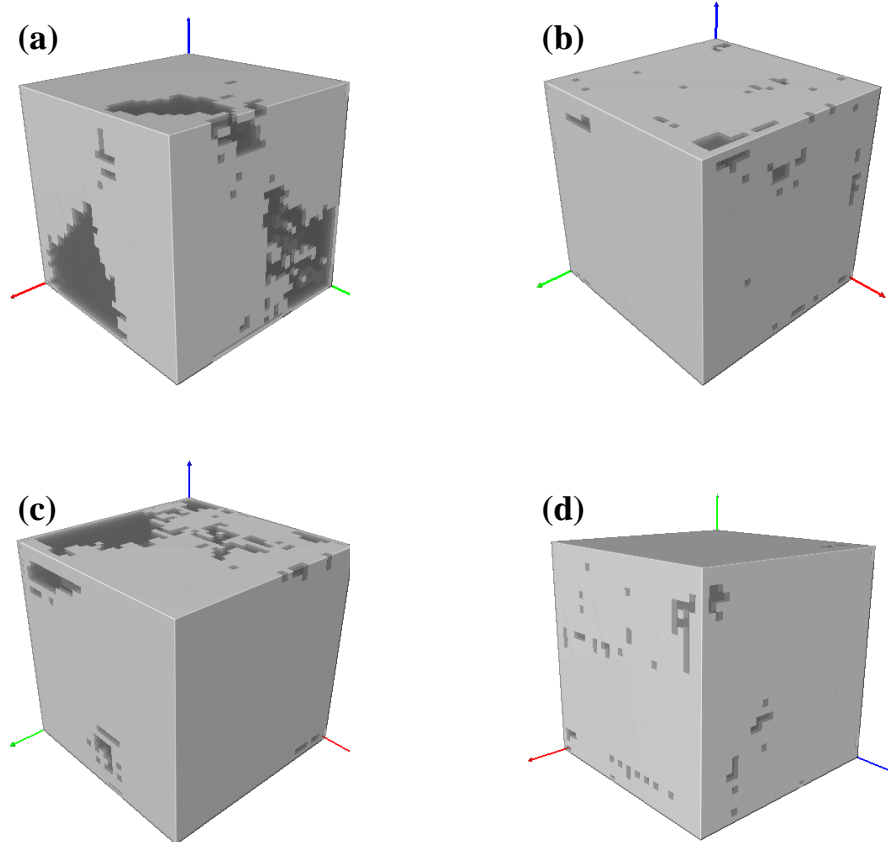429   rock reconstructed by DCGAN.

430

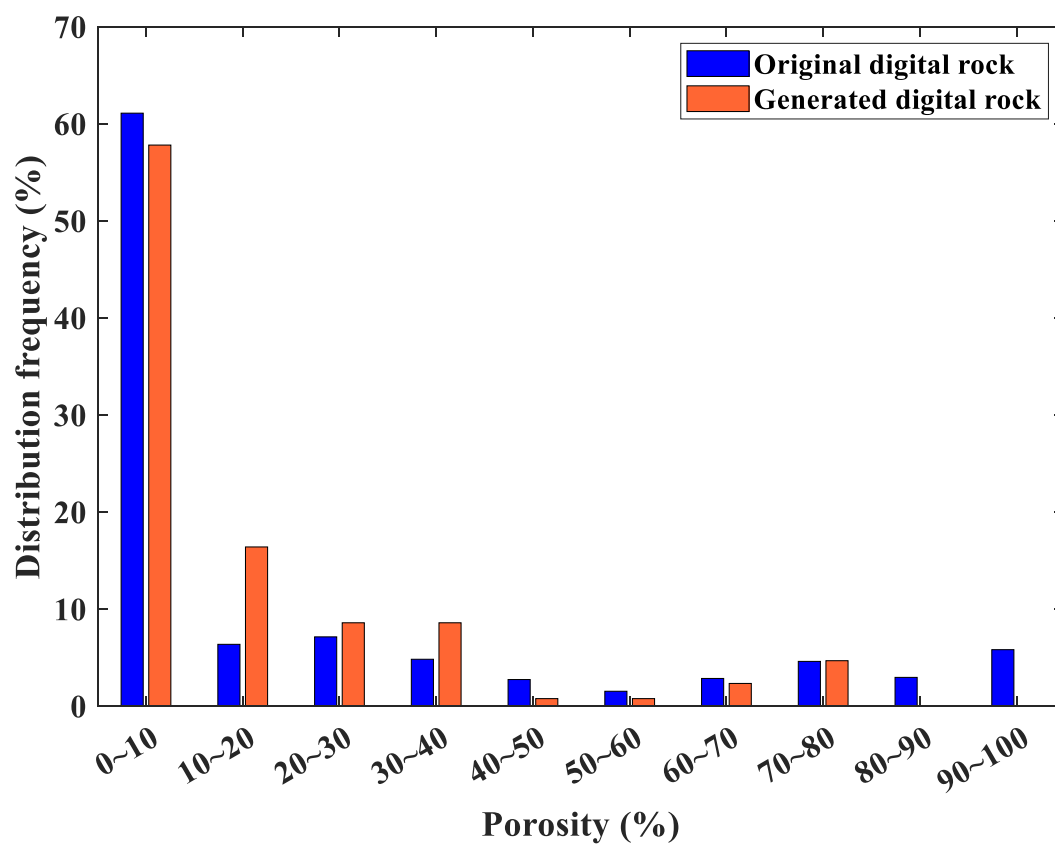**Figure 12** Four generated 3D digital rock reconstructed by DCGAN.

434

Figure 13 Comparison of porosity distribution between original digital rock and the generated digital rock.

437

438

Table 1 the parameter of DAGAN for 3D digital rock reconstruction

Layer			Type	Filter number	Kernel	Stride	Padding	Batchnor-malization	Dropout	Activation
Generator		1	Deconv	64	2×2×2	2	same	Yes	0	ReLU
		2	Deconv	32	2×2×2	2	same	Yes	0	ReLU
		3	Deconv	16	2×2×2	2	same	Yes	0	ReLU
		4	Conv	1	3×3×3	1	same	Yes	0	tanh
Discriminator		1	Conv	8	3×3×3	2	same	Yes	0.25	Leaky ReLU
		2	Conv	16	3×3×3	2	same	Yes	0.25	Leaky ReLU
		3	Conv	32	3×3×3	2	same	Yes	0.25	Leaky ReLU
		4	Conv	64	3×3×3	1	same	Yes	0.25	Leaky ReLU
		5	Fully Connect	4096	-	-	-	-	-	Sigmoid

439

440   **Table 2** Comparison of barycenter coordinates of the pores in the original digital rock and
441   generated digital rock.

Pore no.	Original digital rock			Generated digital rock			Euclidean distance (μm)
	Barycenter coordinate X (μm)	Barycenter coordinate Y (μm)	Barycenter coordinate Z (μm)	Barycenter coordinate X (μm)	Barycenter coordinate Y (μm)	Barycenter coordinate Z (μm)	
1	0.83	0.55	1.94	0.99	0.52	3.28	1.35
2	11.67	2.36	2.04	11.74	2.36	2.17	0.15
3	36.60	0.94	1.97	36.23	0.85	1.83	0.40
4	20.77	10.69	2.78	20.99	10.82	2.63	0.29
5	15.93	31.85	1.56	16.16	31.83	1.60	0.24
6	35.69	26.54	0.31	28.82	22.42	13.88	15.76
7	2.44	1.22	18.30	0.00	1.22	20.74	3.45
8	6.28	23.41	32.04	6.30	23.30	31.99	0.13
9	21.62	3.36	35.49	21.70	3.35	35.48	0.08

442
443

444 **Table 3** The barycenter coordinates of the pores in the original digital rock and generated digital
445 rock.

Label	Original digital rock			Generated digital rock			Euclidean distance (μm)
	Barycenter coordinate X (μm)	Barycenter coordinate Y (μm)	Barycenter coordinate Z (μm)	Barycenter coordinate X (μm)	Barycenter coordinate Y (μm)	Barycenter coordinate Z (μm)	
1	2.00	0.80	1.40	2.00	0.80	1.40	0.00
2	9.60	0.00	0.00	9.60	0.00	0.00	0.00
3	21.58	17.21	20.35	21.58	17.21	20.35	0.00
4	12.00	1.20	0.00	12.00	1.20	0.00	0.00
5	7.60	4.40	0.00	7.60	4.40	0.00	0.00
6	0.00	5.60	0.40	0.00	5.60	0.40	0.00
7	3.60	6.00	0.00	3.60	6.00	0.00	0.00
8	0.00	9.60	0.60	0.00	9.60	0.60	0.00
9	2.40	9.60	0.60	2.40	9.60	0.60	0.00
10	8.40	3.60	6.00	8.40	3.60	6.00	0.00
11	31.20	24.00	12.00	31.20	24.00	12.00	0.00
12	27.60	25.20	37.20	27.60	25.20	37.20	0.00

446